Instability and rupture of ultrathin freestanding viscoelastic solid films

Satya Sekhar, Ashutosh Sharma, and V. Shankar*
Department of Chemical Engineering, Indian Institute of Technology Kanpur, Uttar Pradesh 208016, India

(Received 26 January 2022; accepted 12 August 2022; published 29 August 2022)

We analyze the instability of viscoelastic solid freestanding thin films under the influence of van der Waals forces using linear stability analysis and nonlinear simulations. Linear stability analysis shows that the zero-frequency elastic modulus governs the onset of instability and stabilizes the film beyond a critical value analogous to thin supported viscoelastic solid films. However, for freestanding solid films, the critical shear modulus is found to be independent of surface tension, unlike that of thin supported viscoelastic solid films. It is further shown that freestanding viscoelastic solid films with higher moduli can be destabilized for a given film thickness and Hamaker constant compared to supported solid films. In contrast to thin viscoelastic liquid films where the growth rate is enhanced due to elastic effects but length scale is unaltered, freestanding films with solidlike viscoelasticity show a retarded growth rate and enhanced length scale. The presence of solidlike viscoelasticity has a stabilizing effect and affects all the key aspects of instability such as critical wave number, dominant wave number, and maximum growth rate. We numerically solve the set of coupled nonlinear evolution equations for film thickness and tangential displacement in order to elucidate the dynamics of film rupture. Our simulations show that, consistent with the linear stability predictions, an increase in the elastic modulus delays film rupture. The dynamics exhibits self-similarity in the vicinity of film rupture and the film thins as $(t_r - t)^{3/4}$, where t_r is the rupture time and $t_r - t$ is the time remaining until film rupture. The scaling exponent $3/4$ obtained for a thin freestanding viscoelastic solid film is significantly greater than the scaling exponent $(1/3)$ for a thin freestanding viscous film.

DOI: 10.1103/PhysRevE.106.024803

I. INTRODUCTION

Understanding the instability and dynamics of thin films has received considerable attention owing to its relevance in microfabrication, functional coatings, lab-on-a-chip devices, adhesives, foams and emulsions, etc., and this research area has been extensively reviewed [1–3]. In the biological realm [4–6], stability or integrity of thin films is of interest in contexts such as tear film in the eye [7] and in epithelial layers of the organs [8]. The body of literature that focused on the instability of thin (<100 nm) films can be broadly classified into two categories: thin films resting on a solid substrate (asymmetric or supported films) and thin films bounded by an inviscid fluid (symmetric or freestanding films). Derjaguin [9] first recognized that thin films possess an excess disjoining pressure compared to a bulk liquid. Scheludko [10] proposed that a negative disjoining pressure in the film drives the flow from thinner regions to thicker regions resulting in amplification of interfacial perturbations and film rupture. Vrij [11] calculated the time of rupture and critical thickness of a nondraining freestanding thin liquid film under the influence of van der Waals forces. Ruckenstein and Jain [12] augmented the Navier-Stokes equations with an additional body force term due to van der Waals interactions to study the rupture of both supported and freestanding thin viscous films using linear stability theory within the lubrication approximation. Sharma and Ruckenstein [13] investigated the stability of thin viscous supported and freestanding films subjected to finite amplitude perturbations, i.e., for disturbances with height fluctuations comparable to film thickness.

Linear stability analysis with respect to infinitesimal perturbations is valid only during the initial stage of film rupture, and as the disturbances grow, nonlinearities accelerate the film rupture, which necessitates a more general computational approach to capture the dynamics of film rupture. For thin films, deformations happen on a very large length scale compared to the film thickness, which allows for the use of lubrication approximation to simplify the governing Navier-Stokes equations and boundary conditions in deriving the nonlinear evolution equations. Williams and Davis [14] numerically solved the nonlinear evolution equation for film thickness (derived within the long-wave limit for supported Newtonian thin films) and predicted much shorter rupture times than those inferred from linear stability analysis.

Unlike supported films, freestanding films possess two stress-free interfaces which diminish the viscous resistance to flow [6]. Two different modes of deformation are exhibited by thin free liquid films: squeezing-peristaltic-varicose mode in which the fluctuations in film thickness are symmetric around the centerline, and bending-undulating-sinuous mode in which the film thickness is constant. The squeezing mode leads to the thinning of the film and causes film rupture. Erneux and Davis [15] proposed a different long-wave scaling for a pure freestanding viscous film and obtained a pair of coupled nonlinear evolution equations for film thickness

*Corresponding author: vshankar@iitk.ac.in

and tangential velocity in which the nonlinear contributions of inertial and unsteady terms from the Navier-Stokes equations are retained at higher order in the analysis. The inclusion of inertial or unsteady terms was necessitated because in their absence the length scale of the most unstable mode is infinite in an unbounded system. De Wit *et al.* [16] extended this nonlinear approach to study the stabilizing effect of insoluble surfactants on the rupture of freestanding liquid films and derived three coupled evolution equations for the film thickness, tangential velocity, and surfactant concentration and compared the results with supported liquid films with insoluble surfactants. Their linear stability results show a smaller critical wavelength for a freestanding film than for a supported film. They have also carried out numerical simulations of both systems and showed that supported films need a larger magnitude of van der Waals forces in order to induce the rupture than freestanding films. Sharma *et al.* [17] analyzed the weakly nonlinear evolution of a thin freestanding viscous film devoid of surfactants and numerically solved the set of evolution equations of Erneux and Davis [15] to study the effect of nonlinearities on stability and rupture. Matar [18] examined the influence of soluble surfactants on the dynamics of the rupture of thin freestanding films under the influence of van der Waals forces and has shown through linear stability and nonlinear simulations that instability of the film is promoted by an increase in the degree of surfactant solubility. Lenz and Kumar [19] studied the van der Waals-driven instability of the interior film in a trilayer liquid film system that is confined in a channel with parallel walls, using linear stability analysis and nonlinear simulations. Their results show that a squeezing mode is always a preferred mode of evolution in symmetric configurations, whereas in asymmetric configurations initial growth of instability is dominated by a bending mode of evolution and the squeezing mode takes over close to film rupture.

The aforementioned theoretical studies deal with the stability of rheologically simple, viscous thin liquid films. There has also been considerable amount of research interest to understand the dynamics of thin viscoelastic films. Sathyagal and Narasimhan [20] presented a linear stability analysis to study the rupture of the thin inelastic non-Newtonian power-law liquid film with immobile interfaces under the influence of van der Waals interactions. Tomar *et al.* [21] investigated the instability and rupture of the Jeffreys-type viscoelastic liquid supported film using linear stability and nonlinear simulations. Their results show that liquidlike viscoelasticity merely accelerates the growth rate without affecting the length scale of instability. Sarkar and Sharma [22] presented a general unified theory of field-induced instabilities in thin viscoelastic films. They observed that unlike purely viscous films which are unconditionally unstable for any small destabilizing interaction potential, viscoelastic solid thin films are unstable below a critical film thickness or above critical field strength. The instability, in this case, occurs between two neutral wave numbers and the region of instability shrinks with an increase in elasticity without affecting the dominant wave number. Further, Patra *et al.* [23] investigated the instability engendered by van der Waals forces in thin linear viscoelastic solid films using linear stability analysis and nonlinear simulations.

Barra *et al.* [24] studied the nonlinear evolution of thin Jeffreys viscoelastic film on a solid substrate and investigated the effects of relaxation and retardation characteristic times and the slip coefficient on the dynamics and final configuration of the fluid. Their results show that the length scale of instability is affected neither by rheological parameters nor by slippage coefficient, but all these parameters influence the timescale of instability wherein the maximum growth rate is increased by increase in either relaxation time or slip length but is decreased with the increase in retardation time. Bazzi and Carvalho [25] studied the effect viscoelastic properties of polymer solutions on the stability of a thin freestanding liquid sheet through linear stability analysis and nonlinear simulations and found that the rheological behavior has a strong effect on the growth rate of the disturbance and consequently on the film breakup time. Henkel *et al.* [26] developed a long-wave model to capture the dynamics of a liquid drop on an elastic substrate.

Slippage considerably influences the instability and dynamics of thin films [24,27–36]. The majority of the studies on thin viscous [7,12,14] or viscoelastic [21–23] supported films assume that the film is rigidly bonded to the substrate and employ the no-slip boundary condition. However, substrates which are modified with coatings of self-assembled monolyers [37] or through any surface-grafting techniques [38] provide slip lengths on an order of microns for films with thickness of few tens of nanometers [33,39]. Sippage effects are often incorporated using a Navier-slip boundary condition. Münch *et al.* [29] theoretically investigated the dewetting behavior of fluids on hydrophobic substrates using lubrication models for a wide range of slip lengths. They found that the rim profiles become very asymmetric in the strong-slip regime, which are otherwise symmetrical in the no-slip and weak-slip regimes. Rauscher *et al.* [30] explored the influence of slippage on the dispersion curves and showed that the position of the maximum shifts towards smaller wave numbers for increasing slip length in the strong-slip regime. Xu *et al.* [35] followed an experimental cum theoretical approach to analyze the dynamics of slipping films by modulating the slippage at the confined interface in a PMMA-PS bilayer system. Their experimental findings and a general linear stability analysis reveal that the slip-dominated noncircular morphologies possess a larger interhole spacing than similar nonslipping systems. The experimental study of Lessel *et al.* [34] on the dewetting of polymeric films on lower-energy substrates shows enhanced dewetting dynamics due to presence of strong slip and the film breakup is consistent with the behavior observed in freestanding films.

A freestanding elastomeric film is a case of diverging slip length, and in this article the limiting case of a freestanding viscoelastic solid film is explored. In an earlier study [40], we have carried out a general linear stability analysis of thin freestanding viscoelastic films under the influence of attractive van der Waals forces for different rheologies. In this study, we adopt the approach of Erneux and Davis [15] for the case of a thin freestanding viscoelastic solid film and derive a set of coupled nonlinear equations for the evolution of film thickness and tangential displacement. A linear stability analysis of these nonlinear evolution equations is performed. The dynamics of film rupture is studied through nonlinear

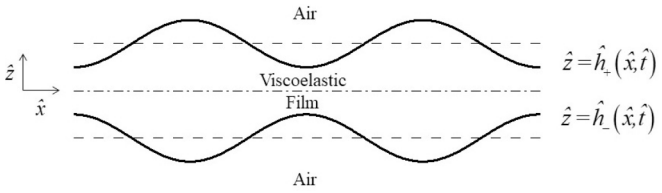

FIG. 1. Schematic representation of an undulating thin freestanding viscoelastic solid film. The dash-dotted line represents the origin of the Cartesian coordinate system, and the film is symmetric around this line. The upper and the lower deforming interfaces of the freestanding film are located at $\hat{z} = \hat{h}_+(\hat{x}, \hat{t})$ and $\hat{z} = \hat{h}_-(\hat{x}, \hat{t})$, respectively. The dashed lines represent the mean positions of the deforming interfaces at $\hat{z} = \pm\hat{h}_0/2$.

simulations. The remainder of this article is organized as follows. A theoretical model of the freestanding solid film is presented in Sec. II. Nondimensional scaling, coupled evolution equations of freestanding film in the long-wave limit, and the details of numerical solution methodology are given in Sec. III. A long-wave dispersion relation is obtained in Sec. IV by linearizing the coupled evolution equations. Section V discusses the results obtained from the linear stability analysis and numerical simulations. A brief summary of the findings from the present study is given in Sec. VI. The details of the derivation of the coupled nonlinear evolutions are provided in the Appendix.

II. THEORETICAL MODEL

Figure 1 shows the schematic of a thin freestanding viscoelastic film of mean thickness $\hat{h}_0$, bounded by a nonviscous medium on either side. The two free surfaces of the film are located at $\hat{z} = \hat{h}_\pm(\hat{x}, \hat{t})$ which undulate around their mean positions at $\hat{z} = \pm\hat{h}_0/2$. Thus, the instantaneous film thickness is given by $\hat{h}^*(\hat{x}, \hat{t}) = \hat{h}_+(\hat{x}, \hat{t}) - \hat{h}_-(\hat{x}, \hat{t})$. A two-dimensional Cartesian coordinate system $(\hat{x}, \hat{z})$ is employed to formulate the present theoretical analysis as shown in Fig. 1. We assume that the film is symmetric in the $\hat{z}$ direction around the centerline. In the following formulation, the variable $\hat{t}$ represents time. Boldface variables denote vector quantities, whereas boldface Greek letters denote tensor quantities. The variables with subscripts represent partial differentiation with respect to the subscripted variable, and the over-dot represents the time derivative.

We consider the film to be a zero-frequency incompressible linear viscoelastic solid. The constitutive relation of the film is given by

$$\hat{\boldsymbol{\tau}} = \hat{G}(\hat{\boldsymbol{\nabla}}\hat{\mathbf{u}} + \hat{\boldsymbol{\nabla}}\hat{\mathbf{u}}^T) + \hat{\mu}(\hat{\boldsymbol{\nabla}}\dot{\hat{\mathbf{u}}} + \hat{\boldsymbol{\nabla}}\dot{\hat{\mathbf{u}}}^T), \tag{1}$$

where a hat denotes a dimensional quantity, and the notations $\hat{\boldsymbol{\tau}}$, $\hat{\mathbf{u}} = (\hat{u}, \hat{w})$, $\hat{G}$, and $\hat{\mu}$ represent the stress tensor, displacement vector, shear modulus, and viscosity of the film, respectively. Here $\hat{u}$ and $\hat{w}$, respectively, represent $\hat{x}$ and $\hat{z}$ components of the displacement vector. Equation (1) represents a Kelvin-Voigt model, which is a linear combination of a Hookean elastic spring and a Newtonian dashpot connected in parallel. Materials such as cross-linked PDMS deforming to a steady-state strain under a constantly applied stress gradually relax to the undeformed state upon removal of stress, with a characteristic timescale determined by the ratio of moduli $(\hat{\mu}/\hat{G})$, and can be described using Eq. (1). This constitutive relation is capable of capturing the interfacial deformations of such materials under the exposure of intermolecular forces or an electrostatic field [23,41,42]. Such instabilities are often within the realm of the small-deformation approximation and well within the limit of linear stability analysis. The nonlinear simulations presented in the present study focus on the interfacial deformations in the long-wave limit, and the present approach should serve the purpose.

In thin films, van der Waals forces become a dominant body force in comparison to gravitational forces. The dynamics of such films can be expressed using the following mass and momentum conservation equations:

$$\hat{\boldsymbol{\nabla}} \cdot \hat{\mathbf{u}} = 0, \tag{2}$$

$$\hat{\rho}\frac{D\dot{\hat{\mathbf{u}}}}{D\hat{t}} = -\hat{\boldsymbol{\nabla}}\hat{p} + \hat{\boldsymbol{\nabla}} \cdot \hat{\boldsymbol{\tau}}. \tag{3}$$

Here the notation $\hat{p} = \hat{p}^* + \hat{\phi}$ is the total pressure, where $\hat{p}^*$ is the pressure in the solid and $\hat{\phi}$ is the conjoining pressure. We enforce symmetry boundary conditions at the centerline $(\hat{z} = 0)$ i.e., a zero normal displacement condition and zero tangential displacement gradient,

$$\hat{w} = 0, \quad \hat{u}_{\hat{z}} = 0. \tag{4}$$

At the film-air interfaces $(\hat{z} = \hat{h}_\pm)$, tangential and normal stress balances are used as boundary conditions along with the kinematic conditions for the free interfaces,

$$\hat{\mathbf{t}} \cdot \hat{\boldsymbol{\tau}} \cdot \hat{\mathbf{n}} = 0, \tag{5}$$

$$-\hat{p}^* + \hat{\mathbf{n}} \cdot \hat{\boldsymbol{\tau}} \cdot \hat{\mathbf{n}} = \pm\hat{\gamma}\hat{\kappa}, \tag{6}$$

$$\dot{\hat{h}}_\pm + \dot{\hat{\mathbf{u}}} \cdot \hat{\boldsymbol{\nabla}}\hat{h}_\pm = \dot{\hat{w}}. \tag{7}$$

Here $\hat{\gamma}$ and $\hat{\kappa}$ are the surface tension and the curvature of the free surface, respectively. The surface tension $\hat{\gamma}$ is assumed to be constant, and thus the shear stresses on the interface vanish. The curvature of the free surface is given by $\hat{\kappa} = \hat{\boldsymbol{\nabla}} \cdot \hat{\mathbf{n}}$. The symbols $\hat{\mathbf{n}}$ and $\hat{\mathbf{t}}$ are the unit outward normal and tangential vectors, which are defined as $\hat{\mathbf{n}} = [\hat{\boldsymbol{\nabla}}(\hat{z} - \hat{h}_\pm)/|\hat{\boldsymbol{\nabla}}(\hat{z} - \hat{h}_\pm)|\ ]$ and $\hat{\mathbf{n}} \cdot \hat{\mathbf{t}} = 0$.

The disjoining-conjoining pressure $\hat{\phi}$ in the total pressure $\hat{p} = \hat{p}^* + \hat{\phi}$ is the excess pressure arising due to attractive van der Waals interactions, which is obtained from the gradient of interaction energy per unit area of the film as shown below:

$$\hat{\phi} = \frac{\partial(\Delta\hat{G})}{\partial\hat{h}^*} = \frac{\hat{A}}{6\pi\hat{h}^{*3}} - \frac{8\hat{B}}{\hat{h}^{*9}}. \tag{8}$$

Here $\hat{A}$ is the Hamaker constant, and $\hat{B}$ is the Born repulsion coefficient, which is introduced to remove the singularity at extremely small thicknesses of the film. The expression for Born repulsion coefficient is obtained by exploiting the minimum free energy condition $[\hat{\phi}(\hat{l}_0) = 0]$ at the cutoff distance $\hat{l}_0 \sim 0.137$ nm [43–45]. We consider the squeezing mode of film deformation, with the interfacial deformation being symmetric about the centerline (i.e., $\hat{h}_+ = \hat{h}_-$). The analysis can therefore be simplified by considering the domain $0 \leqslant \hat{z} \leqslant$

$\hat{h}_+$. Henceforth, the half-film thickness $\hat{h}_+(\hat{x},\hat{t})$ is written as $\hat{h}(\hat{x},\hat{t})$. The intermolecular potential $\hat{\phi}$ in terms of the half-film thickness after incorporating the Born repulsion term is given as [44]

$$\hat{\phi} = \frac{\hat{A}}{6\pi(2\hat{h})^3}\left[1 - \left(\frac{\hat{l}_0}{2\hat{h}}\right)^6\right]. \tag{9}$$

III. LONG-WAVE APPROXIMATION

A. Scales for nondimensionalization

The governing equations and the boundary conditions presented in Sec. II are made dimensionless using the following scales: length (or displacement) $\sim\hat{h}_0$, time $\sim\hat{\rho}\hat{h}_0^2/\hat{\mu}$, velocity $\sim\hat{\mu}/\hat{\rho}\hat{h}_0$, surface tension $\sim\hat{\mu}^2/\hat{\rho}\hat{h}_0$, and shear modulus and pressure $\sim\hat{\mu}^2/\hat{\rho}\hat{h}_0^2$. The nondimensional variables or parameters employing the above scales are $(h, h_\pm) = (\hat{h}, \hat{h}_\pm)/\hat{h}_0$, $(x, z) = (\hat{x}, \hat{z})/\hat{h}_0$, $(u, w) = (\hat{u}, \hat{w})/\hat{h}_0$, $l_0 = \hat{l}_0/\hat{h}_0$, $t = \hat{t}\hat{\mu}/\hat{\rho}\hat{h}_0^2$, $(\dot{u}, \dot{w}) = (\hat{u}, \hat{w})\,\hat{\rho}\hat{h}_0/\hat{\mu}$, $\gamma = \hat{\gamma}\,\hat{\rho}\hat{h}_0/\hat{\mu}^2$, $G = \hat{G}\hat{\rho}\hat{h}_0^2/\hat{\mu}^2$, $(p, p_f, \phi) = (\hat{p}, \hat{p}_f, \hat{\phi})\,\hat{\rho}\hat{h}_0^2/\hat{\mu}^2$, and $A = \hat{A}\hat{\rho}/(6\pi\hat{\mu}^2\hat{h}_0)$.

B. Coupled evolution equations within the long-wave approximation

For deformations occurring over a length scale much larger compared to the mean film thickness, the complete set of governing equations and boundary conditions can be simplified using lubrication approximation [2,12]. To this end, a small parameter $\varepsilon = 2\pi\hat{h}_0/\hat{\lambda}$ is introduced, wherein $\hat{\lambda}$ is the characteristic long length scale of the instability, which is obtained by balancing the surface tension forces with intermolecular attractive interactions to yield $\hat{\lambda} = [6\pi(\hat{h}_0)^4\hat{\gamma}/\hat{A}]^{1/2}$. We use the long-wave scaling introduced by Erneux and Davis [15] in the context of viscous freestanding films:

$$\begin{aligned} &X = \varepsilon x, \quad Z = z, \quad T = \varepsilon^2 t,\\ &\dot{U} = \varepsilon^{-1}\dot{u}, \quad \dot{W} = \varepsilon^{-2}\dot{w}, \quad P = \varepsilon^{-2}p, \quad \Phi = \varepsilon^{-2}\phi,\\ &H = h, \quad \Gamma = \gamma, \quad \bar{G} = \varepsilon^{-2}G, \quad \bar{A} = \varepsilon^{-2}A. \end{aligned} \tag{10}$$

This long-wave scaling enables us to retain the unsteady or inertial terms in the governing equations of thin freestanding films [15–17], whereas those terms are asymptotically small when the governing equations are scaled employing the scaling used for supported films [14].

The nondimensional governing equations and boundary conditions are scaled using the above long-wave scaling given by Eq. (10). The governing equations in terms of the scaled variables are as follows:

$$U_X + W_Z = 0, \tag{11}$$

$$\begin{aligned} &\varepsilon^2(\ddot{U} + \dot{U}\dot{U}_X + \dot{W}\dot{U}_Z)\\ &\quad = -\varepsilon^2(P+\Phi)_X + \bar{G}(\varepsilon^2 U_{XX} + U_{ZZ}) + (\varepsilon^2\dot{U}_{XX} + \dot{U}_{ZZ}), \end{aligned} \tag{12}$$

$$\begin{aligned} &\varepsilon^2(\ddot{W} + \dot{U}\dot{W}_X + \dot{W}\dot{W}_Z)\\ &\quad = -(P+\Phi)_Z + \bar{G}(\varepsilon^2 W_{XX} + W_{ZZ}) + (\varepsilon^2\dot{W}_{XX} + \dot{W}_{ZZ}). \end{aligned} \tag{13}$$

The boundary conditions in terms of the scaled variables are as follows. The symmetry conditions at the center line $Z = 0$ are

$$U_Z = W = 0. \tag{14}$$

The tangential, normal stress balances, and kinematic equation at $Z = H(X,T)$ are

$$\begin{aligned} &\left(1-\varepsilon^2 H_X^2\right)[\bar{G}(U_Z + \varepsilon^2 W_X) + (\dot{U}_Z + \varepsilon^2\dot{W}_X)]\\ &\quad + 2\varepsilon^2 H_X[\bar{G}(W_Z - U_X) + (\dot{W}_Z - \dot{U}_X)] = 0, \end{aligned} \tag{15}$$

$$\begin{aligned} &-P + 2\left(1+\varepsilon^2 H_X^2\right)^{-1}\left\{\left(1-\varepsilon^2 H_X^2\right)(\bar{G}W_Z + \dot{W}_Z)\right.\\ &\quad \left. - H_X[\bar{G}(U_Z + \varepsilon^2 W_X) + (\dot{U}_Z + \varepsilon^2\dot{W}_X)]\right\}\\ &\quad - \Gamma H_{XX}\left(1+\varepsilon^2 H_X^2\right)^{-\frac{3}{2}} = 0, \end{aligned} \tag{16}$$

$$\dot{H} + \dot{U}H_X - \dot{W} = 0. \tag{17}$$

The following perturbation expansion for U, W, and P is introduced in the scaled governing equations and boundary conditions [Eqs. (11)–(17)]:

$$(U, W, P) = (U_0, W_0, P_0) + \varepsilon^2(U_1, W_1, P_1) + \cdots. \tag{18}$$

Note that we have not shown the expansion of the dynamical variable H (the interfacial deflection) because only the leading order contribution to H is required in the present analysis. A pair of coupled nonlinear evolution equations (19) for the half-film thickness and the longitudinal displacement of a thin freestanding viscoelastic solid film are obtained by carrying out a higher order $O(\varepsilon^2)$ analysis of equations of motion. The following set of coupled nonlinear equations can be derived (details given in the Appendix) for the evolution of film thickness and longitudinal displacement:

$$\dot{h} + (h\dot{u})_x = 0, \tag{19a}$$

$$h(\ddot{u} + \dot{u}\dot{u}_x + \phi_x - \gamma h_{xxx}) = 4[(h\dot{u}_x)_x + G(hu_x)_x]. \tag{19b}$$

C. Nonlinear simulations

The two coupled nonlinear evolution equations for freestanding film thickness and longitudinal displacement [Eqs. (19)] are discretized using a central difference scheme with half-node interpolation. The resulting set of stiff coupled ordinary differential equations are solved in time, at each grid point, using Gear's algorithm (using the D02EJF subroutine of NAG library). Periodic boundary conditions are used at the domain boundaries. Initial condition for the film thickness $h(x,t)$ was given as a periodic perturbation with small amplitude around the dimensionless mean half-film thickness, whereas zero tangential displacement is imposed as the initial condition for $u(x,t)$ at all the grid points. Simulations are carried out in a domain sufficiently larger than the wavelength of the fastest growing disturbance. The domain size was chosen as a multiple of $\lambda = \lambda_m$, obtained from the linear stability analysis. The grid independence of the solutions is ensured by varying the number of grid points. Our code is benchmarked with an earlier work [17] on the nonlinear stability of ultrathin freestanding viscous films, as discussed in Sec. V.

TABLE I. Expressions of k_c, k_m, and ω_m for different thin films.

Type of thin film	k_c	k_m	ω_m
Freestanding viscoelastic solid film	$\left(\frac{6A-8G}{\gamma}\right)^{\frac{1}{2}}$	$\left[\frac{(3A-4G)(\gamma-2\sqrt{2\gamma})}{\gamma(\gamma-8)}\right]^{\frac{1}{2}}$	$\frac{(3A-4G)(-4+\sqrt{2\gamma})}{2(\gamma-8)}$
Freestanding viscous film	$\left(\frac{6A}{\gamma}\right)^{\frac{1}{2}}$	$\left[\frac{3A(\gamma-2\sqrt{2\gamma})}{\gamma(\gamma-8)}\right]^{\frac{1}{2}}$	$\frac{3A(-4+\sqrt{2\gamma})}{2(\gamma-8)}$
Supported viscoelastic solid film	$\left(\frac{3A\pm\sqrt{9A^2-4\gamma G}}{2\gamma}\right)^{\frac{1}{2}}$	$\left(\frac{3A}{2\gamma}\right)^{\frac{1}{2}}$	$\left(\frac{9A^2}{4\gamma}\right)-G$

IV. LINEAR STABILITY ANALYSIS

An initially steady viscoelastic film with constant half-film thickness $h=\frac{1}{2}$ is subjected to an infinitesimal disturbance (denoted by primed quantities) of the form $(u,h)=(0,\frac{1}{2})+(u',h')$. The following set of linearized coupled evolution equations are obtained upon introducing these forms in Eqs. (19):

$$\dot{h}'+\frac{1}{2}\dot{u}'_x=0, \tag{20a}$$

$$\ddot{u}'+\phi_h h'_x-\gamma h'_{xxx}-4(G u'_{xx}+\dot{u}'_{xx})=0. \tag{20b}$$

In the linear stability analysis ϕ_h is evaluated at the base state, which is given as $\phi_h=-6A$. We introduce normal modes for h' and u' as follows:

$$(h',u')=(\tilde{h}',\tilde{u}')\,e^{\omega t+ikx}. \tag{21}$$

Here k is the wave number of perturbations, and ω is the growth rate, with the system being unstable if $\mathrm{Re}(\omega)>0$. Substituting the normal modes in the linearized evolutions [Eqs. (20)], we obtain the following dispersion relation:

$$\omega^2+4k^2(\omega+G)+\frac{3}{2}k^2\left(\frac{\gamma}{3}k^2-2A\right)=0. \tag{22}$$

In the dispersion relation, Eq. (22), the last term represents the destabilizing intermolecular interaction force, while the third and the fourth terms are due to the stabilizing elasticity and surface tension of the film, respectively.

The critical wave number k_c is defined such that for $0<k<k_c$ the system is unstable $\omega(k)>0$ and $\omega(k_c)=0$. In the unstable domain, the wave number corresponding to the maximum growth rate is referred to as the dominant wave number k_m. The expressions for k_c, k_m, and ω_m for a thin freestanding viscoelastic film are given in Table I along with the corresponding expressions for thin supported viscoelastic film and thin viscous freestanding film, which are obtained from the long-wave dispersion relations given in the literature [17,23].

From Table I, we can see that the critical wave number of a thin freestanding viscoelastic solid film is always less than that of a thin viscous freestanding film, which indicates the shrinkage in instability domain of the former film. Similarly, we can observe that the dominant wave number of a thin freestanding viscoelastic solid film shifts towards longer wavelengths as the elasticity of a freestanding film increases. In the asymptotic limit of zero shear modulus, the analytical expressions for k_c, k_m, and ω_m of a thin freestanding viscoelastic solid film reduce to the corresponding analytical expressions of a thin freestanding viscous film. The presence of solidlike viscoelasticity exerts a stabilizing influence on the freestanding film and also governs the onset of instability.

The striking difference between thin supported and freestanding viscoelastic films is that in the former case the instability zone is enclosed between two critical wave numbers, and in the latter case there exists a single critical wave number similar to the dewetting of thin viscous supported films or thin viscous freestanding films. For a supported zero-frequency viscoelastic solid film, Patra *et al.* [23] showed that the dominant length scale of instability is influenced neither by viscosity nor by shear modulus but by the surface tension and the film thickness, which is evident from the dominant wave number k_m expression in Table I. However, for a thin freestanding viscoelastic solid film, the dominant wavelength is also a function of shear modulus and viscosity in addition to surface tension and film thickness. There exists a critical shear modulus in both freestanding and supported viscoelastic films below which the instability is predicted for a given film thickness.

Tomar *et al.* [21] showed that liquidlike viscoelasticity of Jeffrey's type does not alter the dominant length scale of instability but aids in accelerating the growth rate. In contrast, the solidlike viscoelasticity for a freestanding film enhances the dominant length scale of instability and retards the growth rate as will be discussed in the linear stability results presented in Sec. V. The dominant wavelength of instability is given as $\lambda_{\mathrm{m}}=2\pi/k_{\mathrm{m}}$. Similarly, for a perturbation of amplitude δ, the linear theory gives the rupture time as $t_{\mathrm{r}}=(1/\omega_{\mathrm{m}})\ln(1/2\delta)$.

V. RESULTS AND DISCUSSION

A. Linear stability results

Sharma *et al.* [17] have shown the variation of growth rate with wave number of a viscous freestanding film in which the retention of an unsteady term [the term proportional to ω^2 in Eq. (22)] in the long-wave dispersion relation leads to the existence of a dominant wave and the omission of which causes the monotonous decrease of growth coefficient with wave number [12]. We first validate our formulation by considering the limit of a purely viscous film, which is obtained by setting $G=0$ in the dispersion relation given by Eq. (22). Figure 2(a) shows the ω vs k plot in the asymptotic limit of zero shear modulus, which matches with the result of Sharma *et al.* [17] for a thin viscous freestanding film ($k_c=0.0245$, $k_m=0.0078$) for the given set of parameters. Figure 2(b) shows ω vs k curves of a thin freestanding viscoelastic solid film at different values of G (curves 1–4). In this plot, it can be seen that the domain of instability gradually shrinks as G

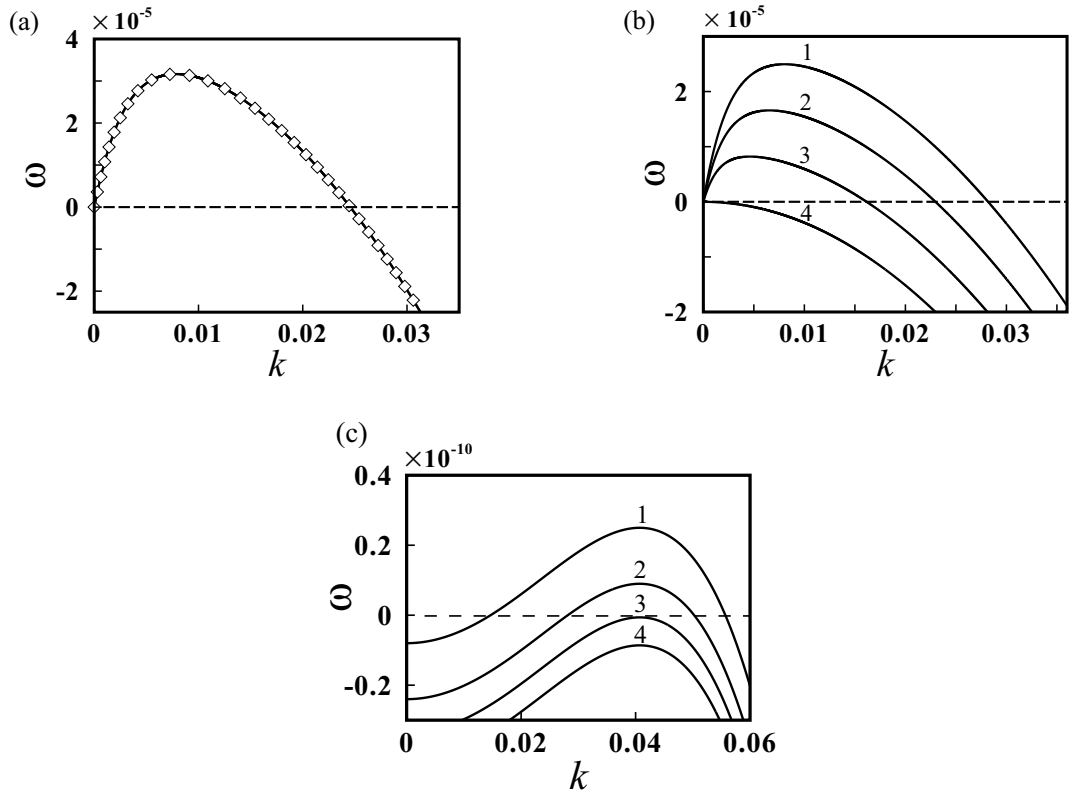

FIG. 2. Linear stability results of thin freestanding and supported viscoelastic solid films. (a) ω vs k curve for a thin freestanding viscoelastic solid film in the asymptotic limit of zero shear modulus (symbols) which matches the ω vs k curve of a thin freestanding viscous film (solid line). (b) ω vs k curves of a thin freestanding viscoelastic solid film. Curves 1–4 correspond to $G = 1 \times 10^{-5}$, 2×10^{-5}, 3×10^{-5}, and 3.98×10^{-5}, respectively. The dimensional parameters used in (a) and (b) are $\hat{h}_0 = 10$ nm, $\hat{\gamma} = 0.0528$ N/m, $\hat{\mu} = 10^{-3}$ Pa s, and $\hat{A} = 10^{-20}$ J. (c) ω vs k curves of a thin supported viscoelastic solid film. Curves 1–4 correspond to $G = 0.8 \times 10^{-11}$, 2.5×10^{-11}, 3.3×10^{-11}, and 4.1×10^{-11}, respectively. The dimensional parameters used in (c) are $\hat{h}_0 = 4$ nm, $\hat{\gamma} = 0.03$ N/m, $\hat{\mu} = 0.1$ Pa s, and $\hat{A} = 10^{-20}$ J.

is increased (curves 1–3). At a certain value of G, the film becomes stable for all the wave numbers (curve 4) and the instability ceases to exist beyond this critical value of G. It can be observed from Fig. 2(b) that incorporating solidlike viscoelasticity affects all the key aspects of the instability such as the cutoff wave number, dominant wave number, and maximum growth rate. Figure 2(c) shows ω vs k dispersion curves of thin supported viscoelastic solid film, which are obtained using the long-wave dispersion relation given by Patra *et al.* [23]. Unlike freestanding solid films, supported solid films exhibit a finite wave number instability. Cross and Hohenberg [46] classified instabilities into different types, according to the nature of linear instability. The instability exhibited by thin supported viscoelastic solid films falls into the category of type I instability in the Cross-Hohenberg classification, whereas the instability exhibited by thin freestanding viscoelastic solid films falls into type II category. The effect of elasticity on the instability of supported viscoelastic solid film is depicted in Fig. 2(c) by plotting the dispersion curves at progressively increasing values of G (curves 1–4). At smaller values of G, curves 1 and 2 lie in the unstable zone and exhibit a band of wave numbers between which the film is unstable. In curve 3, the unstable band of wave numbers reduce to a single wave number (which is also the dominant wave number), where the stabilizing (capillary and elastic) and destabilizing (intermolecular) forces exactly balance. Further increase in G beyond this critical value makes the film stable to all the wave numbers as shown in curve 4. The critical shear modulus (obtained by setting $\omega_m = 0$ in the expression given in Table I) of a thin freestanding viscoelastic solid film below which instability exists is obtained to be $G_c = 3A/4$. Similarly, the critical shear modulus of a thin supported viscoelastic solid film [23], is given as $G_{c,supp} = 9A^2/4\gamma$ below which the film is unstable. The critical shear modulus of a thin freestanding viscoelastic solid film is independent of surface tension, unlike the corresponding supported film. For a given set of parameters, the critical shear modulus of a thin freestanding viscoelastic solid film is much larger than that of a supported solid film. This indicates that relatively harder freestanding viscoelastic films can be destabilized for a given film thickness. In other words, for a given shear modulus relatively thicker freestanding viscoelastic films can be destabilized in comparison with the supported films.

Figure 3 shows the variation of dominant wavelength λ_m and maximum growth rate ω_m of a thin freestanding viscoelastic solid film with film thickness, surface tension, and shear modulus. These parameters are varied one at a time in each plot keeping the remaining parameters constant. In Figs. 3(a)–3(c), the dashed lines show the variation of λ_m and the solid lines show the variation of ω_m with the specific parameter being studied in the plot. Figure 3(a) shows the variation of λ_m and ω_m with A. The parameter A can be increased either

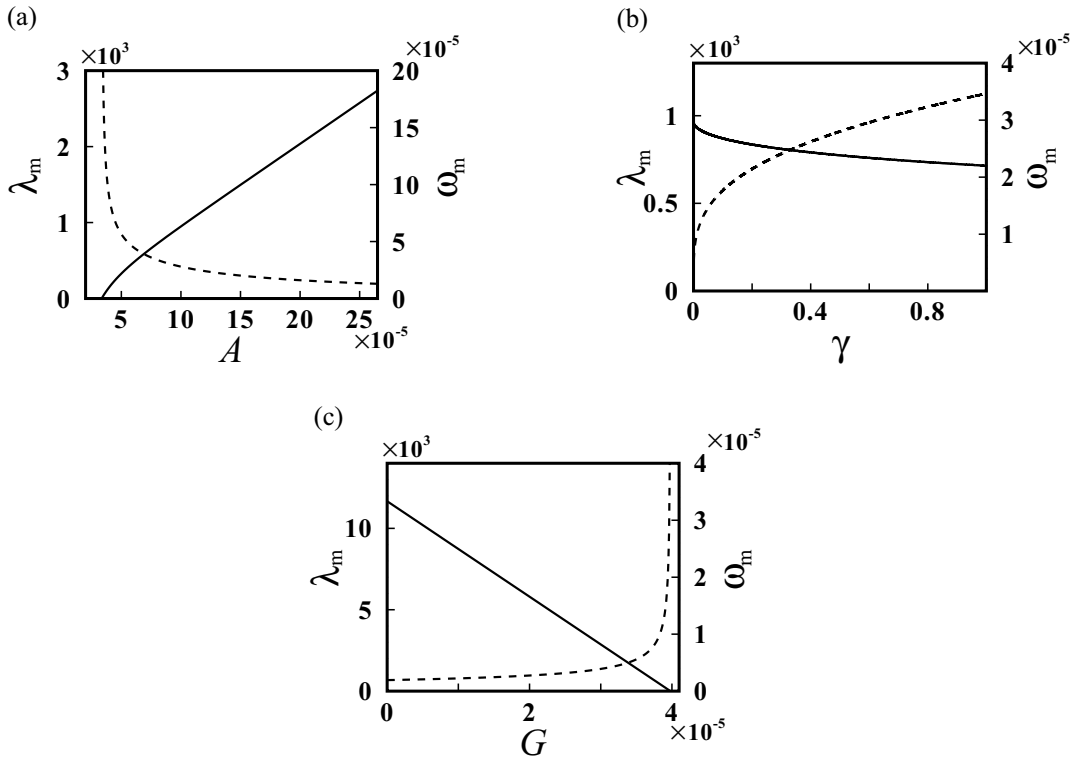

FIG. 3. Effect of various parameters on the dominant wavelength and maximum growth rate of a thin freestanding viscoelastic film. (a) Variation of λ_m and ω_m with A. (b) Variation of λ_m and ω_m with γ. (c) Variation of λ_m and ω_m with G. $\hat{A} = 10^{-20}$ J and $\hat{\mu} = 10^{-3}$ Pa s are common parameters in all the plots. The other three-dimensional parameters ($\hat{h}_0 = 10$ nm, $\hat{\gamma} = 0.03$ N/m, $\hat{G} = 100$ Pa) are varied one at a time in each plot, keeping the remaining two parameters constant. In (a)–(c) the dashed lines show the variation of λ_m, and the solid lines show the variation of ω_m.

by increasing the strength of intermolecular forces (Hamaker constant) or by reducing the film thickness. In Fig. 3(a) the Hamaker constant is kept constant and only the film thickness is varied. It can be seen that dominant wavelength decreases, and growth rate increases with increase in A, which indicates the strengthening of the instability with the decrease in the film thickness. As the film thickness is gradually increased (A is decreased), the dominant wavelength diverges and the maximum growth rate drops to zero upon approaching the critical film thickness. Thus, the instability ceases to exist beyond this critical film thickness. Figure 3(b) shows the variation of λ_m and ω_m with the variation in γ. The stabilizing effect of surface tension is evident from the increase in the dominant wavelength and decrease in the maximum growth rate with increase in the surface tension. Figure 3(c) shows the variation of λ_m and ω_m with G. With an increase in G, the dominant wavelength increases, and it diverges as G_c is approached. Here ω_m decreases linearly with an increase in G and drops to zero at $G = G_c$. Thus, the solidlike viscoelasticity has a stabilizing effect on the instability of thin freestanding viscoelastic solid film, and it also governs the onset of the instability.

Figure 4 compares the dominant wavelength and maximum growth rate of a thin freestanding viscoelastic solid film with that of a thin freestanding viscous film. In Figs. 4(a) and 4(b) the dashed and solid lines correspond to the thin freestanding viscous and viscoelastic films, respectively. In Fig. 4(a) the dominant wavelength of a thin freestanding viscoelastic film is plotted as a function of G. Here the shortest dominant wavelength occurs at $G = 0$, which coincides with the dominant wavelength of a thin freestanding viscous film. The dominant wavelength increases with an increase in G and it diverges as we approach the critical value G_c. This is in contrast to supported viscoelastic films, where the dominant wavelength is unaltered with changes in the elastic modulus. Similarly, Fig. 4(b) shows that a thin freestanding viscoelastic solid film has the highest maximum growth rate at $G = 0$. Here the maximum growth rate decreases linearly with the shear modulus, which becomes zero at $G = G_c$ Thus, the solidlike viscoelasticity retards the growth of the instability of a thin freestanding viscoelastic film.

A bifurcation diagram separates the instability region into stable and unstable zones in the k_c-G plane. The region inside the curve is an unstable zone, and the region outside the curve is a stable zone. Figure 5 compares the bifurcation diagrams of freestanding and supported viscoelastic films having same film thickness for different values of surface tension. Figure 5(a) shows the variation of k_c with G of a thin freestanding viscoelastic solid film. The critical wave number k_c decreases with an increase in G and becomes zero at $G = G_c$. Curves 1–3 correspond to different surface tension values. It is evident from this plot that larger capillary forces diminish the region of instability but do not affect the critical shear modulus G_c, of a thin freestanding viscoelastic solid film. In the unstable

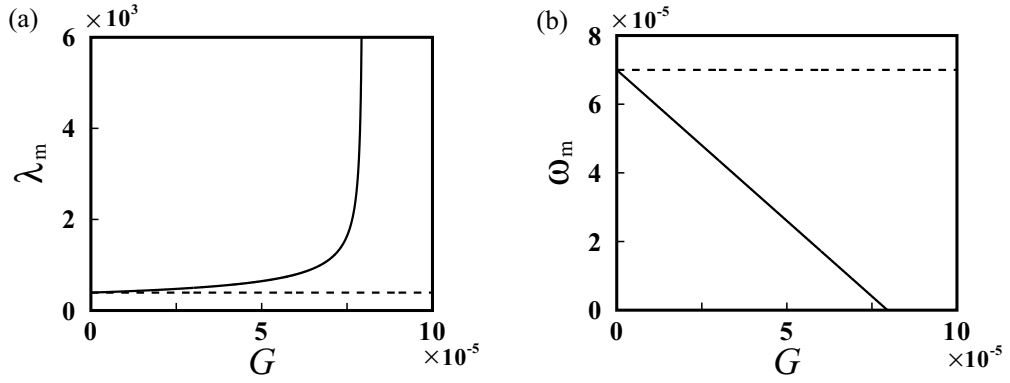

FIG. 4. Comparison of dominant wavelength and maximum growth rate of thin freestanding viscoelastic film with that of thin viscous freestanding film. (a) Variation of λ_m with G. (b) Variation of ω_m with G. In (a) and (b) the solid line refers to freestanding viscoelastic film, and the dashed line refers to freestanding viscous film. The other dimensional parameters used are $\hat{h}_0 = 5$ nm, $\hat{\gamma} = 0.03$ N/m, and $\hat{A} = 10^{-20}$ J.

region, unlike a thin freestanding viscoelastic solid film which has a single critical wave number for a given value of G, Fig. 5(b) shows that a supported solid film has two critical wave numbers between which the instability manifests. As the value of G is increased, at one point these two critical wave numbers merge to a single critical wave number corresponding to the dominant wave number. Unlike freestanding solid films, an increase in the strength of capillary forces not only diminishes the region of instability but also decreases the critical shear modulus in supported solid films. Thus, for a freestanding solid film, G_c depends only on the strength of the destabilizing van der Waals interactions and the film thickness.

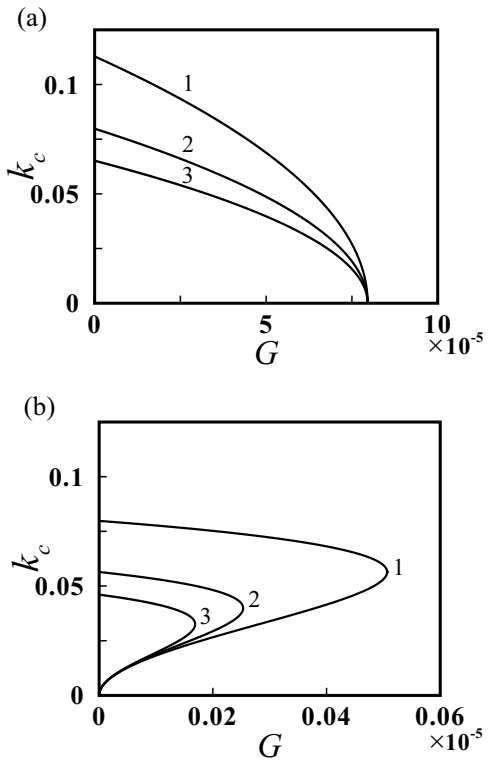

FIG. 5. Bifurcation diagrams of thin freestanding and supported viscoelastic solid films for different values of surface tension. (a) and (b) Variation of k_c with G for a thin freestanding viscoelastic film and thin supported viscoelastic, film respectively. Curves 1–3 in both plots correspond to $\hat{\gamma} = 0.01$, 0.02, and 0.03 N/m, respectively. The other parameter values are $\hat{h}_0 = 5$ nm and $\hat{A} = 10^{-20}$ J.

B. Nonlinear evolution

Initially, the nonlinear simulations are performed for the asymptotic case of a thin freestanding viscous film by keeping the shear modulus at zero ($G = 0$) for the same set of parameters used by Sharma *et al.* [17] for the purpose of validation. The results shown in Fig. 6 show very good agreement between our numerical formulation and earlier results.

Next, we show the effect of elasticity on the morphological evolution and rupture time of thin viscoelastic freestanding film. Figure 7 shows the dynamics of film rupture of a 5 nm thin freestanding viscoelastic solid film in a 3λ domain with an initial sinusoidal perturbation of small amplitude ($\delta = 0.01$) for two different shear moduli below the critical shear modulus. Figures 7(a) and 7(b) show the nonlinear evolution of the half-film thickness (h) of freestanding films. The wavelength of perturbation is chosen to be the dominant wavelength obtained from the linear stability analysis. The perturbation gets amplified and the film ruptures at each minimum of the perturbation. The rupture time t_r is taken as the time at which the minimum film thickness reaches the precursor thickness at any lateral location in the domain under consideration. The freestanding solid film shown in Fig. 7(b) has a higher shear modulus and takes a longer time to rupture in comparison with the film shown in Fig. 7(a), which has a lower shear modulus. The maximum height of the ruptured morphology at the time of film rupture in Figs. 7(a) and 7(b) also indicates that an increase in solidlike elasticity induces stiffness to the freestanding film. Figures 7(c) and 7(d) show the corresponding tangential displacement profiles of these films at the same instants of time where the height evolution profiles are simulated. The film material gets depleted from the regions of minimum thickness and gets accumulated in the regions of maximum thickness. A positive value of u implies the material movement towards right, and a negative value of u indicates the material movement towards left. It can be seen from this

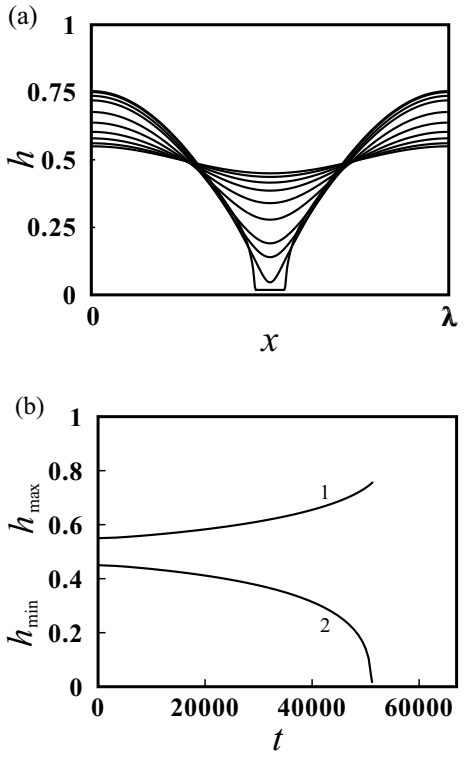

FIG. 6. Nonlinear evolution of a 10 nm thin viscoelastic film for $G = 0$, $\gamma = 0.528$, $\delta = 0.05$. (a) Film profiles at different times ($t = 0$, 10 000, 18 700, 26 600, 35 500, 42 500, 48 000, 49 600, 51 000, 51 200) until rupture occurs. (b) Evolution of the maximum and minimum half-film thicknesses until film rupture. Curves 1 and 2, respectively, show the variation of maximum and minimum half-film thicknesses with time.

figure that a sign change in the displacement happens at each extremum of the half-film thickness h. Further growth of the hole, after the rupture of the thin freestanding viscoelastic solid film (results not shown here), is accompanied by the formation of rims (which should not appear during the hole growth of thin freestanding films [47] due to the absence of friction) similar to the dewetting of thin supported films. In the nonlinear simulations of freestanding films, a small precursor thickness is used to avoid the singularities. This could be the reason for the formation of rims in the postrupture dynamics. Thus, the dynamics of hole growth of thin freestanding films needs more accurate numerical algorithms. Hence, in this article the nonlinear simulation results are confined until the rupture of freestanding film.

Figure 8 shows the time evolution of total pressure in the freestanding film. The expression for pressure profile is given by Eq. (A11) of the Appendix. The corresponding pressure profiles shown in Fig. 8 are for the same conditions given in Fig. 7(a). We can observe from these pressure profiles that the film material depletes from the regions of negative pressure and accumulates in the regions of positive pressure. The pressure in this problem is an adiabatic variable, which is eliminated in the final forms of coupled nonlinear evolution equations, Eqs. (19). The material movement here is essentially governed by the interplay of van der Waals, capillary, and elastic forces.

The influence of shear modulus and surface tension on the rupture time of thin freestanding viscoelastic solid film is studied next. To depict the influence of these parameters, minimum half-film thickness ($h_{\min}$) is plotted as a function of time until the film rupture. Figure 9(a) shows the variation of $h_{\min}$ as a function of t for different shear moduli when the surface tension is kept constant. Among the four different films shown in Fig. 9(a), the one with higher shear modulus exhibits more resistance to film rupture and takes a longer time for film rupture. Thus, the rupture time is enhanced with the increase in shear modulus. Similarly, the variation of $h_{\min}$ with t is shown in Fig. 9(b) for different values of surface tension when the shear modulus is kept constant. Surface tension being a stabilizing force, an increase in its magnitude increases the rupture time and vice versa as can be seen from the four different curves shown in Fig. 9(b). Thus, the thin freestanding viscoelastic solid film ruptures more slowly with either the increase in shear modulus or surface tension. We can also see from Fig. 9 that nonlinearities accelerate the film rupture beyond a certain time.

There have been several studies [48–52] which have elucidated the self-similar nature of the dynamics near rupture for both thin supported and freestanding films of Newtonian and power-law fluids. It is therefore of interest to examine whether self-similar dynamics is present in freestanding solid films, and if so, whether it is similar or different from the other cases studied in the literature. Thus, in addition to the transient solution behavior for thin freestanding solid films, a quantitative analysis of rupture dynamics is also carried out near the film rupture. The rupture dynamics shown in Fig. 9 suggests a possibility for the existence of self-similarity of the solution as the rupture time is approached. Hence, the evolution of minimum half-film thickness h_{min} shown in Fig. 9(a) for different G values is plotted as a function of time remaining until rupture $t_r - t$ on a log-log scale in Fig. 10. Figure 10 shows that the data for different values of G collapse nearly onto a single data set. A scaling law is also estimated which suggests that the film rupture is asymptotically self-similar. The film thickness of thin freestanding solid films for different values of G scales as $(t_r - t)^{3/4}$ near the film rupture, which is shown by the straight line in Fig. 10. Note that this scaling law is different from the one estimated by Vaynblat *et al.* [49] for a thin freestanding viscous film where the film thickness decreases as $(t_r - t)^{1/3}$. Thus, a freestanding viscoelastic solid film ruptures more readily than the viscous film in the regime near the film rupture.

VI. CONCLUSIONS

In the present study, the instability and dynamics of thin freestanding viscoelastic solid films under the influence of destabilizing van der Waals forces have been investigated through linear stability analysis and nonlinear simulations. A set of coupled long-wave nonlinear evolution equations are derived for the film thickness and longitudinal displacement of thin freestanding viscoelastic solid films undergoing squeezing-mode deformation.

The key conclusions from the linear stability analysis are enumerated below:

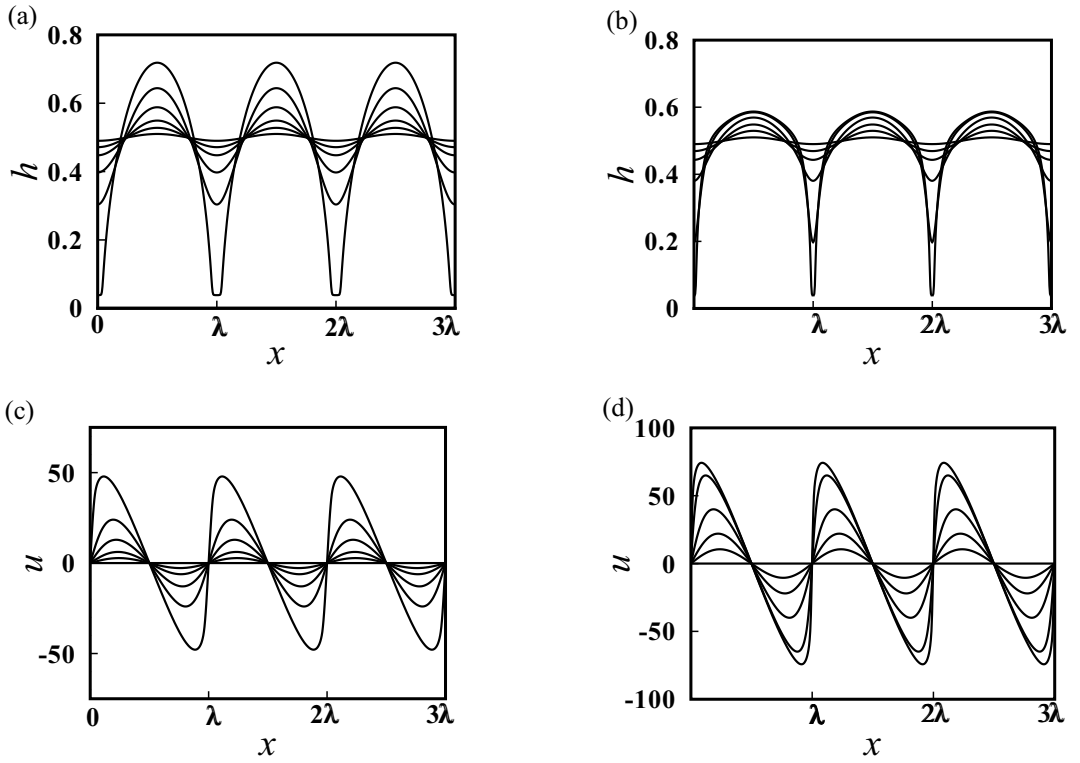

FIG. 7. Nonlinear evolution of thin freestanding viscoelastic solid films until rupture. Panels (a) and (b) show the evolution of the top interface of films with $G = 2.5 \times 10^{-5}$ and $G = 7.5 \times 10^{-5}$, respectively. An initial sinusoidal perturbation of amplitude $\delta = 0.01$ is imposed around the mean film thickness which gets amplified leading to the film rupture. The height evolution profiles shown in plot (a) are at different nondimensional times, $t = 0$, 20 176, 32 437, 45 673, 55 823, and 61 563. Similarly, the successive curves shown in plot (b) are at different nondimensional times, $t = 0$, 45 050, 79 585, 121 095, 141 446, and 143 364. Panels (c) and (d), respectively, show the corresponding tangential displacement profiles, for the films shown in plots (a) and (b), at the same instants of time. The other parameter values are $\hat{h}_0 = 5$ nm, $\hat{\gamma} = 0.03$ N/m, and $\hat{A} = 10^{-20}$ J.

(i) The zero-frequency viscoelasticity in thin freestanding viscoelastic film controls the onset of instability, and the film is unstable below a certain critical shear modulus which is similar to a thin supported viscoelastic film.

(ii) In an unstable thin freestanding viscoelastic solid film, the solidlike viscoelasticity retards the maximum growth rate unlike the liquidlike viscoelasticity, which enhances the maximum growth rate.

(iii) The dominant wavelength of instability increases with the increase in shear modulus of a thin viscoelastic freestanding film. This behavior is different from thin viscoelastic solid- or liquid-supported films where the dominant

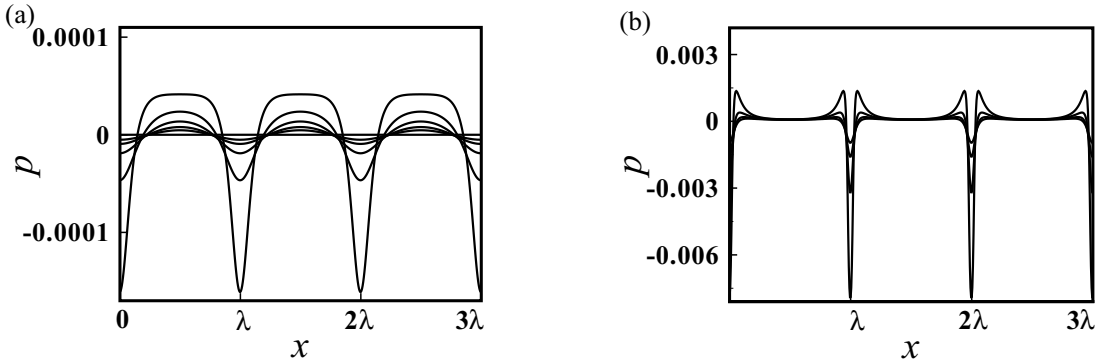

FIG. 8. Pressure profiles during the evolution of thin freestanding viscoelastic solid film. Pressure profiles of early evolution and near to film rupture are shown separately in (a) and (b), respectively. (a) Early evolution: successive curves shown are for different nondimensional times, $t = 0$, 20 176, 32 437, 45 673, and 55 823. (b) Near film rupture: successive curves shown are for different nondimensional times, $t = 60\,574$, 60 916, 61 194, and 61 408. The parameters and initial conditions are same as those given in Fig. 7(a).

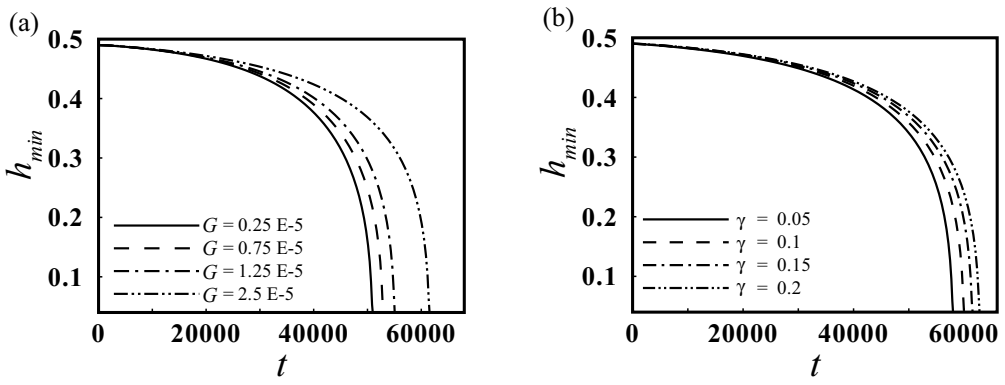

FIG. 9. Effect of elasticity (G) and surface tension (γ) on the rupture time of a thin freestanding viscoelastic solid film. An initial sinusoidal perturbation of amplitude $\delta = 0.01$ is imposed around the mean half-film thickness. (a) $h_{\min}$ vs t at different values of G: 0.25×10^{-5}, 0.75×10^{-5}, 1.25×10^{-5}, and 2.5×10^{-5}. γ is kept constant at 0.15. (b) $h_{\min}$ vs t for different values of γ: 0.05, 0.1, 0.15, and 0.2. G is kept constant at 2.5×10^{-5}. Common parameters used in (a) and (b) are $\hat{h}_0 = 5$ nm and $\hat{A} = 10^{-20}$ J.

wavelength of instability remains invariant to change in shear modulus.

(iv) The critical shear modulus has been found to be independent of surface tension for a thin viscoelastic freestanding film, unlike a thin supported viscoelastic film.

(v) For a given film thickness, the magnitude of critical shear modulus (below which the film is unstable) is much higher for a thin freestanding viscoelastic film than that of a thin supported viscoelastic film, which indicates that much harder viscoelastic freestanding films can be destabilized. In other words, for a given shear modulus, thicker viscoelastic freestanding films can be destabilized more readily than supported viscoelastic films.

The set of coupled nonlinear evolution equations are solved numerically to capture the dynamics of rupture of thin freestanding viscoelastic films. The effect of parameters such as shear modulus and surface tension on the dynamics of film rupture was studied through nonlinear simulations. Simulations show that an increase in either of these parameters slows the dynamics of film rupture. The numerical solution exhibits self-similarity near film rupture, and the minimum half-film thickness of thin freestanding solid films decreases as $(t_r - t)^{3/4}$, where $t_r - t$ is the time remaining until film rupture.

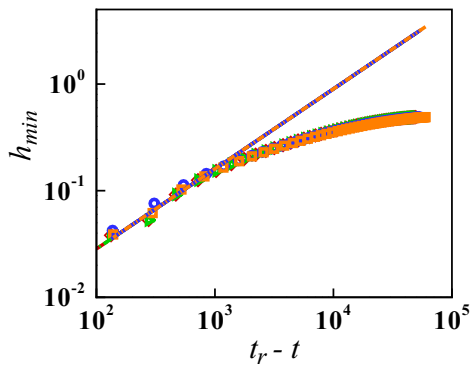

FIG. 10. Variation of the minimum half-film thickness h_{min} with time remaining until rupture $t_r - t$ for the data shown in Fig. 9(a). Thin film evolution data collapse onto a single data set for all four values of G. The minimum half-film thickness of a thin freestanding film is estimated to scale as $(t_r - t)^{3/4}$ near the film rupture. The estimated scaling (collapsed straight lines) closely predicts the evolution of minimum half-film thickness near the rupture, which suggests that the solution exhibits self-similarity.

ACKNOWLEDGEMENT

S.S. thanks Dr. Sivasurender Chandran and Dr. Abir Ghosh for insightful discussions.

APPENDIX: EVOLUTION EQUATIONS OF THIN FREESTANDING VISCOELASTIC SOLID FILM

After incorporating the form of solution sought by Eq. (18), in the scaled governing equations (11)–(13) and the scaled boundary conditions (14)–(16), we obtain the leading order problem by equating ε^2-free terms to zero. At the leading order, we have the following governing equations and boundary conditions.

1. Governing equations

The leading order mass and momentum conservation equations are given by

$$U_{0X} + W_{0Z} = 0, \tag{A1}$$

$$\bar{G}U_{0ZZ} + \dot{U}_{0ZZ} = 0, \tag{A2}$$

$$\bar{G}W_{0ZZ} + \dot{W}_{0ZZ} - (P_0 + \Phi_0)_Z = 0. \tag{A3}$$

2. Boundary conditions

The symmetry condition at $Z = 0$ and the kinematic and normal stress conditions at the free surface are given by: At $Z = 0$

$$U_{0Z} = W_0 = 0. \tag{A4}$$

At $Z = H(X, T)$

$$\bar{G}U_{0Z} + \dot{U}_{0Z} = 0, \tag{A5}$$

$$-P_0 + 2[\bar{G}W_{0Z} + \dot{W}_{0Z} - H_X(\bar{G}U_{0Z} + \dot{U}_{0Z})] = \Gamma H_{XX} \quad \text{(A6)}$$

$$\dot{H} + \dot{U}_0 H_X = \dot{W}_0. \quad \text{(A7)}$$

The X-momentum equation in the leading order [Eq. (A2)] is integrated twice, and one constant of integration is eliminated using the symmetry boundary condition [Eq. (A4)] to get the solution for X displacement in the leading order, which is given as

$$U_0 = C(X, T). \quad \text{(A8)}$$

The continuity equation in leading order [Eq. ((A1)] is integrated once and solved using the symmetry boundary condition [Eq. (A4)] to obtain the Z displacement in the leading order, and after substituting U_0 from Eq. (A8), we get

$$W_0 = -C_X Z. \quad \text{(A9)}$$

Now W_0 is substituted in the leading order Z-momentum equation [Eq. (A3)] and integrated once to get P_0:

$$P_0 = -\Phi_0 - (\bar{G}C_X + \dot{C}_X) + D(X, T). \quad \text{(A10)}$$

Here D is also an unknown function of X and T.

We can observe from the above equation that P_0 is independent of Z, and hence another equation can be obtained for P_0 from the leading order normal stress condition [Eq. (A6)] at the film surface $Z = H(X, T)$:

$$P_0 = -2(\bar{G}C_X + \dot{C}_X) - \Gamma H_{XX}. \quad \text{(A11)}$$

Eliminating P_0 from Eq. (A10) and Eq. (A11) we obtain

$$D(X, T) = \Phi_0 - (\bar{G}C_X + \dot{C}_X) - \Gamma H_{XX}. \quad \text{(A12)}$$

The forms of U_0 and W_0 are substituted into the leading order kinematic equation (A7) to obtain

$$\dot{H} + (H\dot{C})_X = 0. \quad \text{(A13)}$$

Since both H and C are unknown, another relation between them is needed. To obtain this, we analyze the higher order $O(\varepsilon^2)$ problem.

The X-momentum equation in the higher order is

$$(\ddot{U}_0 + \dot{U}_0\dot{U}_{0X} + \dot{W}_0\dot{U}_{0Z}) = -(P_0 + \Phi_0)_X + \bar{G}(U_{0XX} + U_{1ZZ}) + (\dot{U}_{0XX} + \dot{U}_{1ZZ}). \quad \text{(A14)}$$

From the tangential stress balance in the higher order at the film interface at $Z = H(X, T)$ we have

$$\bar{G}(U_{1Z} + W_{0X}) + (\dot{U}_{1Z} + \dot{W}_{0X}) - (\bar{G}U_{0Z} + \dot{U}_{0Z})H_X^2 + 2H_X[\bar{G}(W_{0Z} - U_{0X}) + (\dot{W}_{0Z} - \dot{U}_{0X})] = 0. \quad \text{(A15)}$$

From the symmetry condition at $z = 0$ in higher order, we have

$$U_{1Z} = 0. \quad \text{(A16)}$$

Equation (A14) is integrated once, and using equation Eq. (A16), we obtain

$$(\bar{G}U_{1Z} + \dot{U}_{1Z}) = [\ddot{U}_0 + \dot{U}_0\dot{U}_{0X} + \dot{W}_0\dot{U}_{0Z} + (P_0 + \Phi_0)_X - (\bar{G}\,U_{0XX} + \dot{U}_{0XX})]Z. \quad \text{(A17)}$$

Now U_1 is eliminated from Eqs. (A15) and (A17), and after substituting P_0 from Eq. (A11) we obtain another equation for H and C:

$$H(\ddot{C} + \dot{C}\dot{C}_X + \Phi_{0X} - \Gamma H_{XXX}) = 4[(H\dot{C}_X)_X + \bar{G}(HC_X)_X]. \quad \text{(A18)}$$

Thus, we have two coupled nonlinear equations for film thickness and longitudinal displacement. Finally, we rewrite Eq. (A13) and Eq. (A18) in terms of the original variables to obtain the following evolution equations:

$$\dot{h} + (h\dot{u})_x = 0, \quad \text{(A19a)}$$

$$h(\ddot{u} + \dot{u}\dot{u}_x + \phi_x - \gamma h_{xxx}) = 4[(h\dot{u}_x)_x + G(hu_x)_x]. \quad \text{(A19b)}$$

[1] G. Reiter, Unstable thin polymer films: Rupture and dewetting processes, Langmuir **9**, 1344 (1993).

[2] A. Oron, S. H. Davis, and S. G. Bankoff, Long-scale evolution of thin liquid films, Rev. Mod. Phys. **69**, 931 (1997).

[3] R. V. Craster and O. K. Matar, Dynamics and stability of thin liquid films, Rev. Mod. Phys. **81**, 1131 (2009).

[4] C. Maldarelli, R. K. Jain, I. B. Ivanov, and E. Ruckenstein, Stability of symmetric and unsymmetric thin liquid films to short and long wavelength perturbations, J. Colloid Interface Sci. **78**, 118 (1980).

[5] C. Maldarelli and R. K. Jain, The linear, hydrodynamic stability of an interfacially perturbed, transversely isotropic, thin, planar viscoelastic film: I. General formulation and a derivation of the dispersion equation, J. Colloid Interface Sci. **90**, 233 (1982).

[6] D. S. Dimitrov, Dynamic interactions between approaching surfaces of biological interest, Prog. Surf. Sci. **14**, 295 (1983).

[7] A. Sharma and E. Ruckenstein, An analytical nonlinear theory of thin film rupture and its application to wetting films, J. Colloid Interface Sci. **113**, 456 (1986).

[8] S. Douezan and F. Brochard-Wyart, Dewetting of cellular monolayers, Eur. Phys. J. E **35**, 34 (2012).

[9] B. V. Derjaguin, The definition and magnitude of disjoining pressure and its role in the statics and dynamics of thin liquid films, Kolloid Zh. **17**, 207 (1955).

[10] A. Sheludko, Thin liquid films, Adv. Colloid Interface Sci. **1**, 391 (1967).

[11] A. Vrij, Possible mechanism for the spontaneous rupture of thin, free liquid films, Discuss. Faraday Soc. **42**, 23 (1966).

[12] E. Ruckenstein and R. K. Jain, Spontaneous rupture of thin liquid films, J. Chem. Soc. Faraday Tras. II **70**, 132 (1974).

[13] A. Sharma and E. Ruckenstein, Finite-amplitude instability of thin free and wetting films: Prediction of lifetimes, Langmuir **2**, 480 (1986).

[14] M. B. Williams and S. H. Davis, Nonlinear theory of film rupture, J. Colloid Interface Sci. **90**, 220 (1982).

[15] T. Erneux and S. H. Davis, Nonlinear rupture of free films, Phys. Fluids **5**, 1117 (1993).

[16] A. D. Wit, D. Gallez, and C. I. Christov, Nonlinear evolution equations for thin liquid films with insoluble surfactants, Phys. Fluids **6**, 3256 (1994).

[17] A. Sharma, C. S. Kishore, S. Salaniwal, and E. Ruckenstein, Nonlinear stability and rupture of ultrathin free films, Phys. Fluids **7**, 1832 (1995).

[18] O. K. Matar, Nonlinear evolution of thin free viscous films in the presence of soluble surfactant, Phys. Fluids **14**, 4216 (2002).

[19] R. D. Lenz and S. Kumar, Instability of confined thin liquid film trilayers, J. Colloid Interface Sci. **316**, 660 (2007).

[20] A. N. Sathyagal and G. Narsimhan, On rupture of a thinning film of non-Newtonian power law liquid, Chem. Eng. Commun. **111**, 161 (1992).

[21] G. Tomar, V. Shankar, S. K. Shukla, A. Sharma, and G. Biswas, Instability and dynamics of thin viscoelastic liquid films, Eur. Phys. J. E **20**, 185 (2006).

[22] J. Sarkar and A. Sharma, A unified theory of instabilities in viscoelastic thin films: From wetting to confined films, from viscous to elastic films, and from short to long waves, Langmuir **26**, 8464 (2010).

[23] A. Patra, D. Bandyopadhyay, G. Tomar, A. Sharma, and G. Biswas, Instability and dewetting of ultrathin solid viscoelastic films on homogeneous and heterogeneous substrates, J. Chem. Phys. **134**, 064705 (2011).

[24] V. Barra, S. Afkhami, and L. Kondic, Interfacial dynamics of thin viscoelastic films and drops, J. Non-Newtonian Fluid Mech. **237**, 26 (2016).

[25] M. S. Bazzi and M. S. Carvalho, Effect of viscoelasticity on liquid sheet rupture, J. Non-Newtonian Fluid Mech. **264**, 107 (2019).

[26] C. Henkel, J. H. Snoeijer, and U. Thiele, Gradient-dynamics model for liquid drops on elastic substrates, Soft Matter **17**, 10359 (2021).

[27] S. Herminghaus, R. Seemann, and K. Jacobs, Generic Morphologies of Viscoelastic Dewetting Fronts, Phys. Rev. Lett. **89**, 056101 (2002).

[28] C. Redon, J. B. Brzoska, and F. Brochard-Wyart, Dewetting and slippage of microscopic polymer films, Macromolecules **27**, 468 (1994).

[29] A. Münch, B. A. Wagner, and T. P. Witelski, Lubrication models with small to large slip lengths, J. Eng. Math. **53**, 359 (2005).

[30] M. Rauscher, R. Blossey, A. Münch, and B. Wagner, Spinodal dewetting of thin films with large interfacial slip: Implications from the dispersion relation, Langmuir **24**, 12290 (2008).

[31] A. Sharma and K. Kargupta, Instability and dynamics of thin slipping films, Appl. Phys. Lett. **83**, 3549 (2003).

[32] K. Kargupta, A. Sharma, and R. Khanna, Instability, dynamics, and morphology of thin slipping films, Langmuir **20**, 244 (2004).

[33] S. Chandran and G. Reiter, Transient Cooperative Processes in Dewetting Polymer Melts, Phys. Rev. Lett. **116**, 088301 (2016).

[34] M. Lessel, J. McGraw, O. Bäumchen, and K. Jacobs, Nucleated dewetting in supported ultra-thin liquid films with hydrodynamic slip, Soft Matter **13**, 4756 (2017).

[35] L. Xu, D. Bandyopadhyay, P. D. S. Reddy, A. Sharma, and S. W. Joo, Giant slip induced anomalous dewetting of an ultrathin film on a viscous sublayer, Sci. Rep. **7**, 14776 (2017).

[36] D. Peschka, S. Haefner, L. Marquant, K. Jacobs, A. Münch, and B. Wagner, Signatures of slip in dewetting polymer films, Proc. Natl. Acad. Sci. USA **116**, 9275 (2019).

[37] P. Gutfreund, O. Bäumchen, R. Fetzer, D. van der Grinten, M. Maccarini, K. Jacobs, H. Zabel, and M. Wolff, Solid surface structure affects liquid order at the polystyrene–self-assembled-monolayer interface, Phys. Rev. E **87**, 012306 (2013).

[38] S. Ma, X. Zhang, B. Yu, and F. Zhou, Brushing up functional materials, NPG Asia Mater. **11**, 24 (2019).

[39] R. Fetzer and K. Jacobs, Slippage of Newtonian liquids: Influence on the dynamics of dewetting thin films, Langmuir **23**, 11617 (2007).

[40] S. Sekhar and V. Shankar, Instability of ultrathin viscoelastic freestanding films, Phys. Fluids **33**, 032115 (2021).

[41] S. Kumar and O. K. Matar, Dewetting of thin liquid films near soft elastomeric layers, J. Colloid Interface Sci. **273**, 581 (2004).

[42] A. Ghosh, D. Bandyopadhyay, and A. Sharma, Influence of the mutable kinetic parameters on the adhesion and debonding of thin viscoelastic films, J. Colloid Interface Sci. **477**, 109 (2016).

[43] C. J. V. Oss, M. K. Chaudhury, and R. J. Good, Interfacial Lifshitz-van der Waals and polar interactions in macroscopic systems, Chem. Rev. **88**, 927 (1988).

[44] R. Khanna and A. Sharma, Pattern formation in spontaneous dewetting of thin apolar films, J. Colloid Interface Sci. **195**, 42 (1997).

[45] A. Ghatak, R. Khanna, and A. Sharma, Dynamics and morphology of holes in dewetting of thin films, J. Colloid Interface Sci. **212**, 483 (1999).

[46] M. C. Cross and P. C. Hohenberg, Pattern formation outside of equilibrium, Rev. Mod. Phys. **65**, 851 (1993).

[47] G. Debrégeas, P. Martin, and F. Brochard-Wyart, Viscous Bursting of Suspended Films, Phys. Rev. Lett. **75**, 3886 (1995).

[48] W. W. Zhang and J. R. Lister, Similarity Solutions for Capillary Pinch-Off in Fluids of Differing Viscosity, Phys. Rev. Lett. **83**, 1151 (1999).

[49] D. Vaynblat, J. R. Lister, and T. P. Witelski, Rupture of thin viscous films by van der Waals forces: Evolution and self-similarity, Phys. Fluids **13**, 1130 (2001).

[50] S. S. Thete, C. Anthony, O. A. Basaran, and P. Doshi, Self-similar rupture of thin free films of power-law fluids, Phys. Rev. E **92**, 023014 (2015).

[51] S. S. Thete, C. Anthony, P. Doshi, M. T. Harris, and O. A. Basaran, Self-similarity and scaling transitions during rupture of thin free films of Newtonian fluids, Phys. Fluids **28**, 092101 (2016).

[52] V. Garg, P. M. Kamat, C. R. Anthony, S. S. Thete, and O. A. Basaran, Self-similar rupture of thin films of power-law fluids on a substrate, J. Fluid Mech. **826**, 455 (2017).